Hartree-Fock studies of atoms in strong magnetic fields

Matthew D. Jones,[1] Gerardo Ortiz,[2] and David M. Ceperley[1]
[1]*National Center for Supercomputing Applications, Department of Physics, University of Illinois at Urbana-Champaign, 1110 West Green Street, Urbana, Illinois 61801*
[2]*Department of Physics, University of Illinois at Urbana-Champaign, 1110 West Green Street, Urbana, Illinois 61801*
(Received 17 November 1995)

We present comprehensive calculations of the electronic structure of selected first-row atoms in uniform magnetic fields of strength $\leqslant 10^{10}$ G, within a flexible implementation of the Hartree-Fock formalism. Ground-state and low-lying excited state properties are presented for first-row atoms He, Li, C, and ion H^-. We predict and describe a series of ground-state quantum transitions as a function of magnetic field strength. Due to its astrophysical importance, highly excited states of neutral He are also computed. Comparisons are made with previous works, where available.

PACS number(s): 32.60.+i, 31.10.+z, 97.10.Ld, 95.30.Ky

I. INTRODUCTION

The behavior of atoms in very strong magnetic fields is not a topic limited only to theoretical interest. Studies of atoms under these extreme conditions first intensified with observations of excitons in semiconductors with small effective masses and large dielectric constants [1], which result in very large effective magnetic fields. For a time, standard perturbative methods [2], valid only in relatively small magnetic fields, were sufficient for understanding these systems. Work on quantum dots [3], observations of neutron stars possessing fields in excess of 10^{12} G [4], and the detection of magnetic white dwarf stars with megagauss fields [5] has further increased interest in this area. Our theoretical knowledge of the behavior of these systems has not kept pace with the experimental work, however, and accurate calculations for multielectron atoms do not exist in the range of magnetic fields encountered in these systems. It is the primary goal of this work to help fill that gap. In a regime where Coulomb and magnetic effects are of nearly equal importance, and neither can be treated as a perturbation, lie many interesting applications, both in astrophysics and condensed matter physics. Unfortunately, this regime is also very difficult to solve, since the combination of the cylindrical symmetry of the magnetic field and the spherical symmetry of the Coulomb potential prevents the Schrödinger equation from being separable and integrable. Previous approaches to this problem have been concentrated on the two limits, very weak magnetic fields (where the magnetic field may be treated as a perturbation), and very strong magnetic fields (where cylindrical symmetry is imposed on the wave function in the so-called adiabatic approximation [6]). Several recent works, however, have attempted to bridge this gap and deal with the intermediate (or strong field) regime. We can work in dimensionless atomic units by introducing $\beta_Z = e a_0^2 B/2\hbar c Z^2 = B/B_0 Z^2$, where $B_0 = 4.7\times 10^9$ G, a_0 is the Bohr radius, and Z is the atomic charge. Depending on the relative strength between Coulomb and magnetic forces, we can characterize three different regimes: the low ($\beta_Z \leqslant 10^{-3}$), the intermediate (strong) ($10^{-3} \leqslant \beta_Z \leqslant 1$), and high (super-strong) ($\beta_Z \gg 1$) field regimes.

Rosner *et al.* [7] have used the numerical Hartree-Fock (HF) method to calculate many states of the hydrogen atom ($Z=1$) in fields up to $\beta_Z \leqslant 10^3$. In these computations, the wave function is expanded in terms of either spherical harmonics or Landau-like orbitals (adiabatic basis set) depending on the field strength, and the resulting Hartree-Fock equations are then integrated numerically. This set of computed energies and oscillator strengths has been used to identify many spectral features of compact stellar remnants, and is often used as a benchmark for other methods [8].

For systems involving more than one electron, efforts have largely been concentrated on the high field (adiabatic) regime, where the magnetic forces dominate, and the wave function is assumed to have cylindrical symmetry. Mueller *et al.* [9] used cylindrical trial wave functions to compute variational upper bounds for the lowest energy states of H^-, He, and Li^+ in the adiabatic approximation for fields in excess of 10^{10} G. Vincke and Baye [10] also obtained variational estimates for H^- and He for magnetic fields in excess of 10^{10} G. Again in the adiabatic limit, with fields larger than 10^{11} G, Miller and Neuhauser [11] and Neuhauser *et al.* [12] have used HF methods on small atoms and molecular chains. Work at such strong magnetic fields, while not complete, is made somewhat easier by the dominance of the magnetic field in this regime. Cylindrical symmetry may be assumed for the mathematical form of the desired wave function in this asymptotic regime. The situation at intermediate fields is more complex.

At intermediate field strengths, the nearly equal importance of Coulomb and magnetic effects has made progress very difficult, and thus far only two electron problems have been attempted. This range of field strengths is plagued by the fact that neither the spherical symmetry of the Coulombic potential nor the cylindrical symmetry of the constant magnetic field may be assumed to dominate. Thorough HF calculations using the same method as Rosner's hydrogenic calculations [7] have been performed for heliumlike atoms [13], but these results, as we shall see, have difficulty in the region where the cylindrical and spherical expansions meet. Less complete variational calculations were performed for H^- by Henry *et al.* [14] ($\beta_Z < 0.2$), and for He by Surmelian *et al.* [15] for $\beta_Z < 20$. Both sets of variational calculations used a trial wave function which was a sum of slater orbitals.

Larsen [16] also performed variational calculations on several low-lying excited states of H^- and He for various fields of $\beta_Z \leqslant 5$, paying particular attention to the binding energy of H^-. A treatment of diatomic hydrogen was carried out by Ortiz *et al.* [17] using quantum Monte Carlo (QMC) methods in fields ranging from $\beta_Z = 0.1$ to $\beta_Z \simeq 200$. We have studied multielectron atoms in this intermediate regime, using a basis set HF approach that is flexible enough to balance the competing symmetries between the Coulomb and magnetic interactions. This work is the precursor of a QMC study of electron correlation at high magnetic fields in atomic systems. The QMC method requires high quality trial wave functions, hence our immediate need for the calculations presented here. At the same time, the method and tables presented here may be of some use to astrophysicists analyzing unexplained spectra from magnetic white dwarf stars, for example GD229, for which helium has been suggested as a possible explanation for the pronounced yet nonhydrogenic spectral features [18].

II. HARTREE-FOCK APPROACH TO ATOMS IN MAGNETIC FIELDS

The Hamiltonian in atomic units for an atom in constant magnetic field is given by

$$\hat{\mathbb{H}} = \sum_{i=1}^{N} \left[-\frac{\nabla_i^2}{2} - \frac{Z}{r_i} + \frac{(Z^2\beta_Z)^2}{2}(x_i^2 + y_i^2) \right] + Z^2\beta_Z(L_z + 2S_z) + \sum_{1 \leqslant i < j \leqslant N} \frac{1}{r_{ij}}, \tag{1}$$

where $L_z = \Sigma_{i=1}^{N} \ell_{iz}$ and $S_z = \Sigma_{i=1}^{N} s_{iz}$ are the z component of the total angular momentum and spin of the system, respectively, and lengths are in units of the Bohr radius a_0. We have chosen the magnetic field to be parallel to the z axis, and the symmetric gauge, which has vector potential $\mathbf{A} = B(-y, x, 0)/2$. In the absence of external fields the eigenvalues of L^2, L_z, S^2, S_z, and parity, Π, are good quantum numbers. When the magnetic field is turned on, the rotational invariance is broken and the only conserved quantum numbers are the eigenvalues of L_z, S^2, S_z, and Π (alternatively, we will use the z parity, Π_z). With a different choice of gauge, L_z no longer commutes with $\hat{\mathbb{H}}$; instead one must use a gauge-covariant form [17]. We will still use L^2 to characterize atomic orbitals coming from solutions of the Hamiltonian, even though L^2 is not a conserved quantity. Although we are using the convenient spectroscopic notation provided by the L^2 operator ($s, p, d, \ldots$), we are in no way biasing our results by imposing the L^2 symmetry—it is simply a bookkeeping tool for tracking the electronic states over a range of magnetic field strengths that includes zero field. The diamagnetic term in the Hamiltonian couples states that differ by two in l. In large fields, for example, our labeling an electronic state as $1s$ denotes the first state of even parity $s + d + g + \cdots$, which would be the familiar $1s$ state at zero field. Taking our wave function to be a single Slater determinant and minimizing the energy of the above Hamiltonian with respect to the electronic spin orbitals, $\{\psi_a\}$ [$\psi_a(\mathbf{x}) = \alpha(s) \otimes \phi_a(\mathbf{r})$, where $\alpha(s)$ is a spin function, $\phi_a(\mathbf{r})$ a spatial orbital, and $\mathbf{x} = (s, \mathbf{r})$], we obtain the usual Hartree-Fock equations,

$$F\psi_a = \epsilon_a \psi_a, \tag{2}$$

where F is the single-particle Fock operator,

$$F = h(\mathbf{r}) + \sum_b (\mathscr{J}_b - \mathscr{K}_b), \tag{3}$$

and

$$h(\mathbf{r}) = -\frac{1}{2}\nabla^2 - \frac{Z}{r} + \frac{(Z^2\beta_Z)^2}{2}(x^2 + y^2) + Z^2\beta_Z(l_z + 2s_z),$$

$$\mathscr{J}_b\psi_a = \left[\int d\mathbf{x}' |\mathbf{r} - \mathbf{r}'|^{-1/2} \psi_b^*(\mathbf{x}') \psi_b(\mathbf{x}') \right] \psi_a(\mathbf{x}),$$

$$\mathscr{K}_b\psi_a = \left[\int d\mathbf{x}' |\mathbf{r} - \mathbf{r}'|^{-1/2} \psi_b^*(\mathbf{x}') \psi_a(\mathbf{x}') \right] \psi_b(\mathbf{x}). \tag{4}$$

Note that we are still considering the integrals over the spin degrees of freedom for the direct, $\mathscr{J}$, and exchange, $\mathscr{K}$, integrals. Rather than integrate the Hartree-Fock equations numerically on a radial grid, we choose to expand each electronic orbital in a basis set, $\{\chi_\mu(\mathbf{r})\}$, of our choosing,

$$\phi_a(\mathbf{r}) = \sum_{\mu=1}^{M} c_{a\mu}\chi_\mu(\mathbf{r}), \tag{5}$$

where M is the number of basis set elements. This expansion reduces the problem to an algebraic one, upon which well established and robust solution methods can be brought to bear. One is also free to choose the dominant symmetry for a given magnetic field regime. At large fields we can use cylindrical basis functions (Landau-like orbitals), while at lower fields strengths it is more advantageous to use basis elements with spherical symmetry. For the intermediate range of magnetic field strength considered here, we have chosen to use Slater-type orbitals (STO) as our basis elements, which have the form

$$\chi_\mu = R_\mu(r) Y_{l_\mu m_\mu}(\theta, \phi), \tag{6}$$

where $R_\mu(r) = N_\mu r^{n_\mu - 1} e^{-a_\mu r}$, $Y_{l_\mu m_\mu}$ are the usual spherical harmonics, and $N_\mu = [(2a_\mu)^{(2n_\mu+1)}/(2n_\mu)!]^{1/2}$ is the normalization constant. Note that this basis-set formulation has a distinct advantage over the direct radial-grid integration method in this particular application of atoms in magnetic fields. With direct integration of the HF equations [Eq. (2)], one must make an assumption about the symmetry of the wave function to reduce the partial differential equation to a more manageable (one-dimensional) ordinary one. At intermediate field strengths, neither cylindrical nor spherical symmetry dominates, making such an assumption hazardous. With the basis-set formalism, one can simply add more basis elements of different symmetry in a systematic way. In practice, we optimize the exponents, $\{a_\mu\}$, of the basis functions using a conjugate gradient approach, then attempt to saturate any remaining freedom in the basis with additional basis

elements. One should also note that the STO basis is complete for any field strength, even if many terms of higher order in l must be included. This advantage is not shared by the adiabatic basis set, in which the wave function is assumed to possess cylindrical symmetry. The individual matrix elements for the STO basis, even in magnetic fields, are straightforward [19], with the exception of the electron-electron interaction. We discuss our method for computing these integrals in the Appendix.

We will use two different approaches to this Hartree-Fock problem, which differ in their assumptions about the initial Slater determinant used in the minimization step above. The first is spin-restricted Hartree-Fock (RHF), in which spin orbitals are pure space-spin products to be occupied in pairs, with a common spatial orbital factor. The second method is spin-unrestricted (UHF), in which the orbitals corresponding to different spins are allowed to differ. Although UHF generally obtains a better variational energy than RHF for open shell configurations, UHF wave functions, unlike their RHF counterparts, are not eigenstates of S^2. For trial wave functions in QMC, it is desirable to begin with eigenstates of S^2, even though a broken symmetry state could have a lower variational energy. One could also project out an eigenstate of spin from the unrestricted calculations, but this additional step presents a needless complication. We will briefly outline the approach that we have taken for using UHF and RHF.

The UHF method is formally much simpler than that of RHF. We have an eigenvalue problem for orbitals of each spin type,

$$\hat{f}^{\alpha}(\mathbf{r})\phi_a^{\alpha}(\mathbf{r}) = \epsilon_a^{\alpha}\phi_a^{\alpha}(\mathbf{r}),$$

$$\hat{f}^{\beta}(\mathbf{r})\phi_a^{\beta}(\mathbf{r}) = \epsilon_a^{\beta}\phi_a^{\beta}(\mathbf{r}), \tag{7}$$

TABLE I. UHF energies for H^-, in hartree. The results from a numerical quadrature solution to the HF equations are from Thurner *et al.* [13], E_{Th}, and the variational calculations of Larsen [16], E_{lar}, are also included. E_{Lar} includes electron correlation, so it should be compared with the Monte Carlo results [22], E_{MC}. Note that the Monte Carlo approach is slightly different, depending on the state; the $1s^2$ state used diffusion Monte Carlo (DMC), while the $1s2p_{-1}$ state used fixed-phase Monte Carlo (FPMC).

β_Z	$E_{UHF}(1s^2)$	$E_{UHF}(1s2p_{-1})$	E_{Th}	E_{Lar}	E_{MC}
0.0001	0.4879	0.5001	0.5001		
0.0005	0.4879	0.5004	0.5004		
0.0010	0.4879	0.5008	0.5008		0.5286(10) $1s^2$
0.0030	0.4879	0.5025	0.5023		
0.0070	0.4876	0.5063	0.5053		
0.0100	0.4873	0.5091	0.5076		0.5270(6) $1s^2$
0.0300	0.4826	0.5280	0.5234		
0.0500	0.4742	0.5460	0.5399	0.549(1)	
0.0700	0.4629	0.5656	0.5569		
0.1000	0.4417	0.5934	0.5823	0.598(1)	0.5965(4) $1s2p_{-1}$
0.2000	0.3472	0.6803	0.6587		
0.3000	0.2308	0.7537	0.7201		0.7606(6) $1s2p_{-1}$
0.4000	0.1011	0.8177			
0.5000		0.8729	0.8094	0.880(1)	0.8821(6) $1s2p_{-1}$
0.6000		0.9223			
0.7000		0.9684	0.8699		0.9766(9) $1s2p_{-1}$
0.8000		1.0101			
0.9000		1.0492			
1.0000		1.0863	0.9980		1.0778(6) $1s2p_{-1}$
1.1000		1.1162			
1.2000		1.1467			
1.3000		1.1877			
1.4000		1.2175			
1.5000		1.2463			
1.6000		1.2723			
1.7000		1.2987			
1.8000		1.3236			
1.9000		1.3464			
2.0000		1.3688	1.3036		
2.1000		1.3918			
2.2000		1.4158			
2.3000		1.4397			
2.4000		1.4602			
2.5000		1.4811			

where $\hat{f}(\mathbf{r})$ is the single-body operator,

$$\hat{f}^{\alpha}(\mathbf{r}_1)\phi_a^{\alpha}(\mathbf{r}_1)=h(\mathbf{r}_1)\phi_a^{\alpha}(\mathbf{r}_1)+\sum_{b=1}^{N_\alpha}[J_b^{\alpha}-K_b^{\alpha}]\phi_a^{\alpha}(\mathbf{r}_1)+\sum_{b=1}^{N_\beta}J_b^{\beta}\phi_a^{\alpha}(\mathbf{r}_1), \tag{8}$$

and α and β denote the two possible spin species ($s=1/2$). To obtain the UHF solutions, one introduces a basis and solves simultaneously the coupled equations for the two spin types.

In the RHF approach, there are two important cases to be considered, closed electronic shells and open shells. The closed shell RHF technique, developed as an algebraic problem with basis set expansions by Roothaan [19], is one of the simplest to implement, but suffers from limited applicability (due to the relative prevalence of open shell systems). For closed electronic shells, one solves

$$\hat{f}\phi_a(\mathbf{r})=h(\mathbf{r})\phi_a(\mathbf{r})+\sum_{b=1}^{N/2}[2J_b-K_b]\phi_a(\mathbf{r}), \tag{9}$$

TABLE II. UHF Energies for low-lying He states, in hartree. E_{Th} are the values reported for numerical quadrature [13].

	$1s^2$	$1s2s$		$1s2p_0$		$1s2p_{-1}$	
β_Z	$-E_{UHF}$	$-E_{UHF}$	$-E_{Th}$	$-E_{UHF}$	$-E_{Th}$	$-E_{UHF}$	$-E_{Th}$
0.0000	2.8617	2.1742		2.1314		2.1314	
0.0001	2.8617	2.1751	2.1751	2.1323	2.1322	2.1326	2.1326
0.0005	2.8617	2.1782	2.1782	2.1354	2.1354	2.1374	2.1374
0.0010	2.8617	2.1821	2.1821	2.1394	2.1394	2.1433	2.1433
0.0030	2.8616	2.1972	2.1972	2.1547	2.1547	2.1659	2.1659
0.0070	2.8611	2.2245	2.2244	2.1834	2.1833	2.2076	2.2076
0.0100	2.8604	2.2429	2.2426	2.2035	2.2032	2.2365	2.2363
0.0300	2.8504	2.3381	2.3306	2.3198	2.3150	2.3992	2.3973
0.0500	2.8310	2.4112	2.3821	2.4196	2.4056	2.5366	2.5312
0.0700	2.8030	2.4771	2.4114	2.5102	2.4842	2.6606	2.6516
0.1000	2.7468	2.5712	2.4266	2.6347	2.5866	2.8299	2.8138
0.1200		2.6331		2.7114		2.9343	
0.1400		2.6934		2.7842		3.0330	
0.1600		2.7517		2.8534		3.1266	
0.1800		2.8084		2.9196		3.2161	
0.2000		2.8632		2.9828	2.8394	3.3017	3.2540
0.2200		2.9169		3.0435		3.3840	
0.2400		2.9690		3.1017		3.4631	
0.2600		3.0194		3.1580		3.5384	
0.2800		3.0682		3.2113		3.6117	
0.3000	2.0923	3.1127		3.2641	3.0033	3.6839	3.5948
0.4000		3.3303		3.5048		4.0096	
0.5000	1.1762	3.5114	2.9340	3.7141	3.1728	4.2950	4.1016
0.6000		3.7001		3.8997		4.5502	
0.7000	0.1275	3.8778	3.3381	4.0698	3.5665	4.7853	4.4658
0.8000		4.0296		4.2207		5.0016	
0.9000		4.1671		4.3595		5.1976	
1.0000	-0.168	4.2891	3.8231	4.4861	4.0609	5.3793	4.9350

TABLE III. UHF energies, $-E_{UHF}$, for low-lying states of Li, in hartree.

β_Z	$1s^22s$	$1s^22p_{-1}$	$1s2s2p_{-1}$	$1s2p_02p_{-1}$
0.0000	7.4327	7.3651	5.3583	5.2318
0.0001	7.4337	7.3669	5.3625	5.2355
0.0005	7.4371	7.3738	5.3767	5.2497
0.0010	7.4412	7.3832	5.3943	5.2673
0.0030	7.4553	7.4114	5.4617	5.3352
0.0070	7.4739	7.4565	5.5837	5.4599
0.0100	7.4814	7.4832	5.6656	5.5455
0.0300	7.4731	7.5965	6.0844	6.0159
0.0500	7.4240	7.6563	6.3993	6.3956
0.0700	7.3609	7.6820	6.6720	6.7284
0.1000	7.2446	7.6747	7.0403	7.1711
0.1200		7.6459	7.2826	7.4404
0.2000	6.6640	7.3627	8.1159	8.3564
0.2200		7.2722	8.3165	8.5578
0.2400		7.1655	8.5075	8.7526
0.2600		7.0391	8.6767	8.9371
0.2800		6.9050	8.8375	9.1160
0.3000	5.8772	6.7747	9.0035	9.2755

where we have performed the integral over spin for $\mathscr{J}$ and $\mathscr{K}$, denoting the resulting direct and exchange spatial integrals J and K. After introducing a basis for the orbitals, one solves the resulting matrix equation for the coefficients $\{c_{a\mu}\}$. This simple sum over direct and exchange contributions when each orbital is doubly occupied becomes more complex in the open shell case. For open shell RHF, many different approaches have been formulated [20]. We have settled on an approach based on that of Guest and Saunders

TABLE IV. UHF energies, $-E_{UHF}$, for low-lying states of C, in hartree.

β_Z	$S_z=-1$	$S_z=-2$	$S_z=-3$
0.0001	37.689	37.312	26.329
0.0005	37.701	37.380	26.439
0.0010	37.743	37.456	26.565
0.0030	37.793	37.728	26.982
0.0070	38.134	38.183	27.644
0.0100	38.325	38.470	28.059
0.0300	38.713	39.598	30.331
0.0500	38.376	40.193	32.035
0.0700	37.677	40.327	33.277
0.1000	36.239	40.361	35.092
0.1200	35.196	40.240	36.089
0.1400		39.983	36.842
0.1600		39.628	37.680
0.1800		39.283	38.154
0.2000	29.969	38.661	39.323
0.2200		38.055	39.726
0.2400		37.370	40.473
0.2600		36.676	41.042
0.2800		35.895	
0.3000	21.472	35.068	

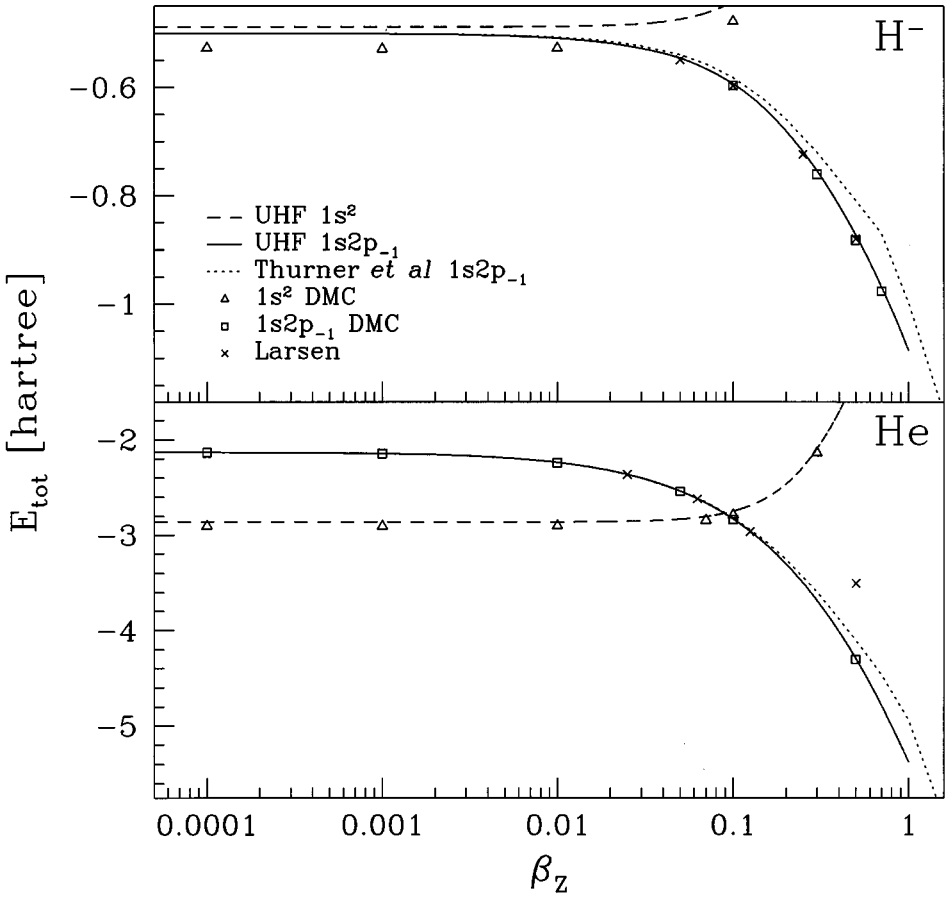

FIG. 1. Ground-state energy of the H^- ion (top) and the He atom (bottom) as a function of magnetic field strength, determined by several different methods. The solid and dashed lines are UHF data of the present work. Crosses are variational calculations of Larsen [16], while the dotted line represents the HF data of Thurner *et al.* [13]. Open squares and triangles are the QMC data of Jones and Ortiz [22].

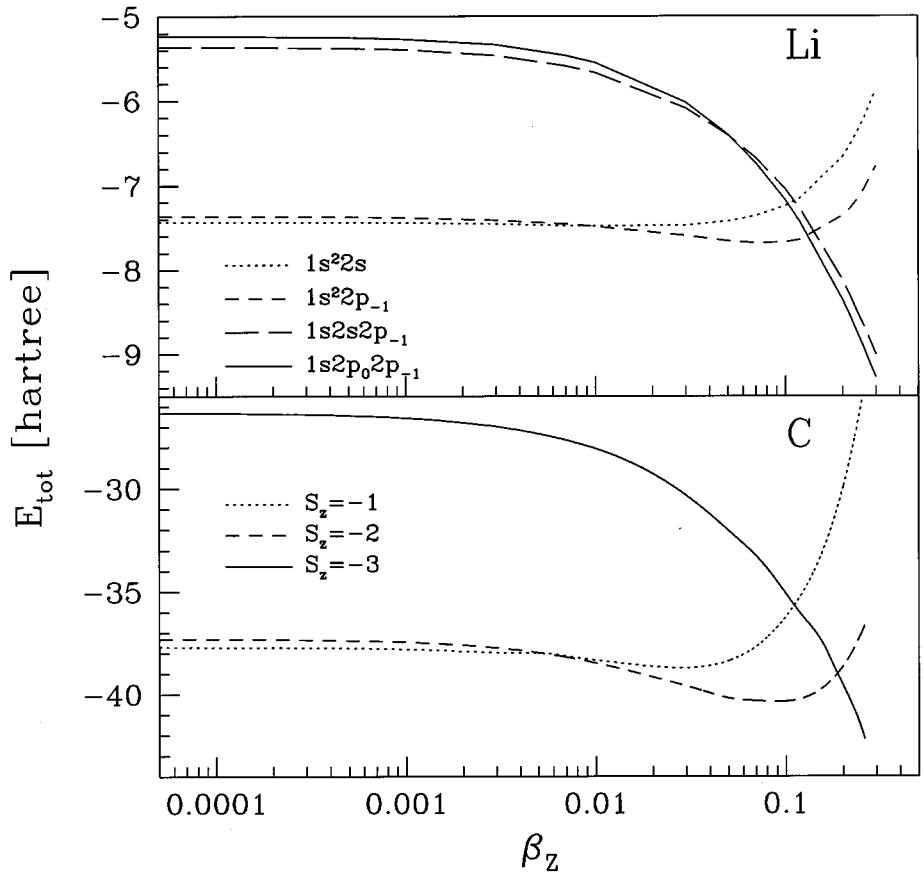

FIG. 2. Ground-state energies of neutral Li (top) and C (bottom) as a function of magnetic field strength. Note the transitions to states of various spin polarization as the field increases.

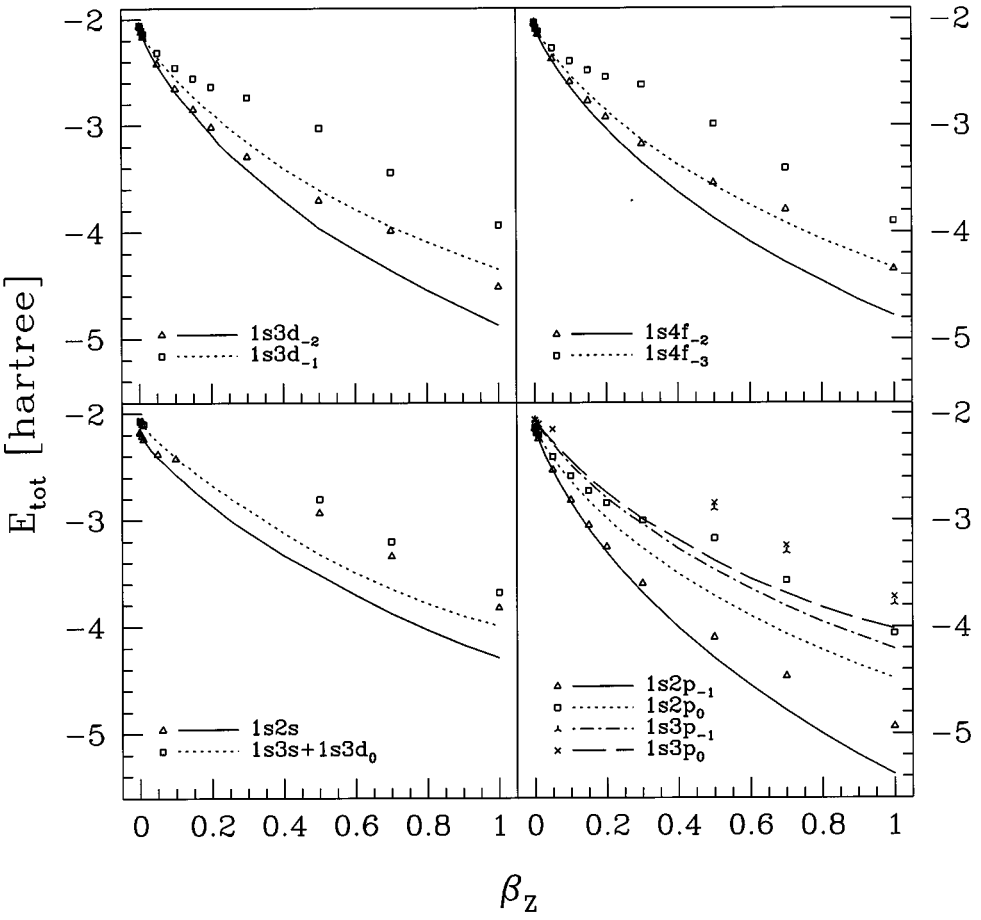

FIG. 3. Energies of some excited states of neutral He. The points represent the data of Thurner *et al.* [13], while the curves show our data. The present results obtain a lower variational energy for all excitations in the range of fields considered here, $0 \leqslant \beta_Z \leqslant 1$.

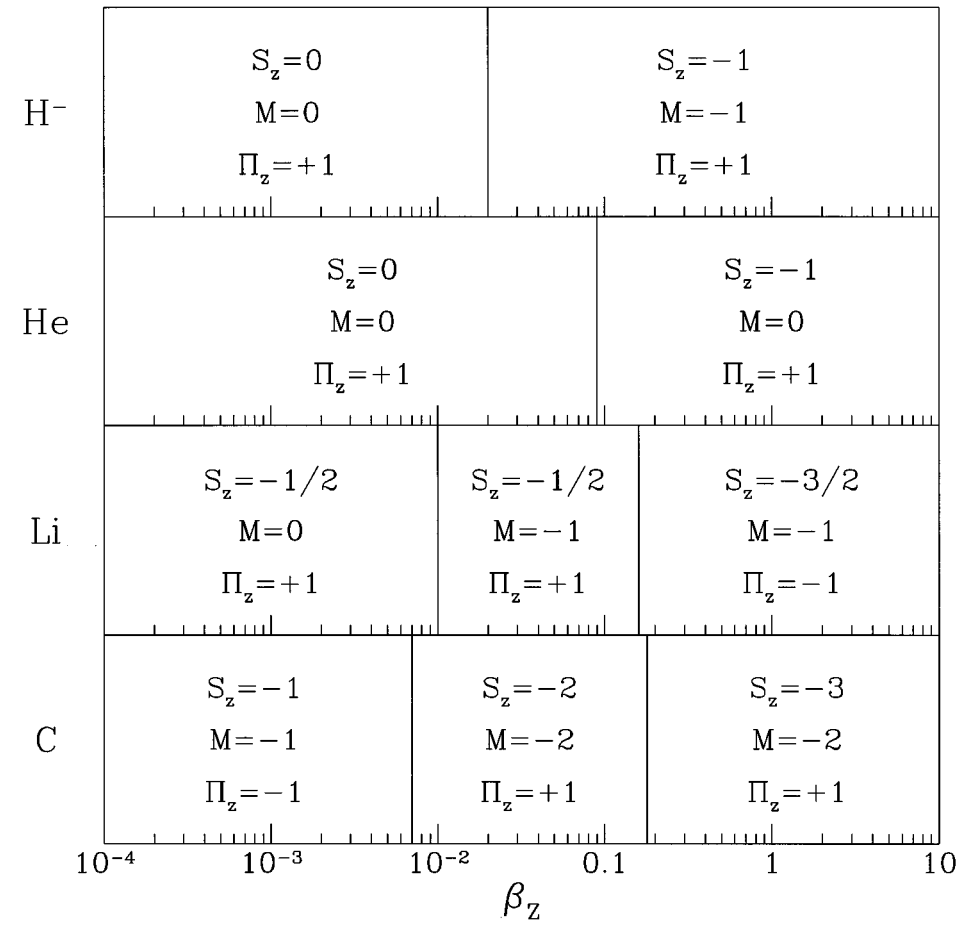

FIG. 4. HF ground-state quantum numbers as a function of magnetic field for the first-row atoms and ion considered in the present work; H^-, He, Li, and C.

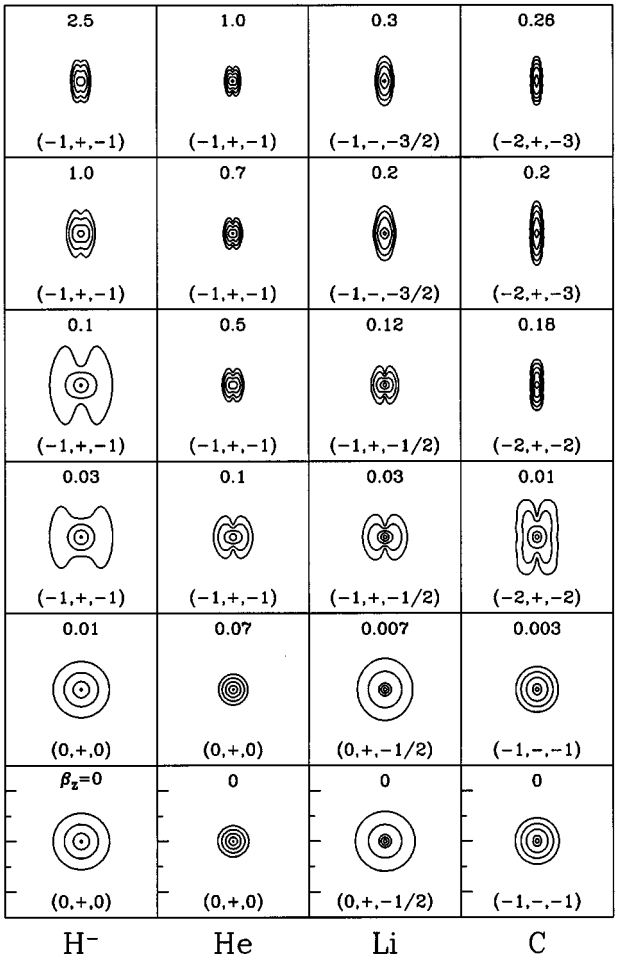

FIG. 5. HF electron densities for the ground-state configuration for H^-, He, Li, and C. The field is in the plane of the page, in the vertical direction. Field strength is given by the number at the top of each panel, and the triplet of numbers at the bottom of each set of contour lines represents the quantum numbers (M,Π_z,S_z). The dimensions of the boxes are the same for abscissa and ordinate, with the scale in Bohr radii, a_0, indicated on the leftmost axis. The large ticks correspond to ten bohr radii. The contour lines are drawn at the same values of the electron density for each atom, and for all field strengths.

[21], which has the advantage of allowing for easier convergence to excited states. This method formulates a generalized matrix such that convergence is obtained when the matrix elements between occupied and unoccupied orbitals vanish. If T_1, T_2, and T_3 denote matrices whose columns are eigenvectors representing closed, open, and empty orbitals, respectively, then let

$$\overline{H}=\begin{pmatrix} T_1^\dagger H_d T_1 & \lambda_{12} T_1^\dagger H_3 T_2 & \lambda_{13} T_1^\dagger H_1 T_3 \\ \lambda_{12} T_2^\dagger H_3 T_1 & T_2^\dagger H_p T_2+\delta_1 I & \lambda_{23} T_2^\dagger H_2 T_3 \\ \lambda_{13} T_3^\dagger H_1 T_1 & \lambda_{23} T_3^\dagger H_2 T_2 & T_3^\dagger H_v T_3+(\delta_1+\delta_2) I \end{pmatrix}, \tag{10}$$

TABLE V. RHF energies for excited He $M=0$ states, in hartree. The results from Thurner *et al.* [13] are given by E_{Th}.

	$1s3s+1s3d_0$		$1s3p_0$	
β_Z	$-E_{RHF}$	$-E_{Th}$	$-E_{RHF}$	$-E_{Th}$
0.0000	2.0685		2.0576	
0.0001	2.0693	2.0693	2.0584	2.0584
0.0005	2.0723	2.0723	2.0615	2.0615
0.0010	2.0758	2.0758	2.0651	2.0651
0.0030	2.0869	2.0863	2.0774	2.0771
0.0070	2.1052	2.0961	2.0969	2.0930
0.0100	2.1179	2.1035	2.1094	2.1007
0.0300	2.1927	2.1381	2.1906	2.1148
0.0500	2.2615	2.1487	2.2701	
0.0700	2.3220		2.3383	
0.1000	2.4071		2.4401	
0.1200	2.4694		2.5112	
0.1400	2.5122		2.5675	
0.1600	2.5723		2.6335	
0.1800	2.6199		2.6885	
0.2000	2.6746		2.7447	
0.2200	2.7192		2.7947	
0.2400	2.7606		2.8468	
0.2600	2.8177		2.8966	
0.2800	2.8555		2.9439	
0.3000	2.8969		2.9932	
0.4000	3.1186		3.1847	
0.5000	3.3228	2.8034	3.3786	2.8405
0.6000	3.4927		3.5505	
0.7000	3.6475	3.2012	3.6908	3.2392
0.8000	3.7841		3.8196	
0.9000	3.9005		3.9324	
1.0000	3.9942	3.6796	4.0202	3.7183

where I is the identity matrix, λ_{ij}, δ_1, and δ_2 are arbitrary parameters to improve convergence, and H_n $(n=1,2,3,d,p,v)$ is an Hermitian matrix whose form depends on the electronic configuration [21]. To obtain self-consistent solutions for the orbitals, one begins with a trial set of solutions, then repeats the process of computing and diagonalizing H until convergence is achieved. This method for converging open shell RHF solutions is very flexible due to the rather large number of free parameters in Eq. (10), and the explicit decoupling of occupied and unoccupied orbitals.

With UHF one does not need elaborate procedures to accommodate different open shell situations; all electronic configurations are treated within the same formalism as given above in Eqs. (7). We have used UHF for all of the ground-state calculations performed in this work, and RHF for the higher excited states of neutral He. The reason behind this choice of method is stability; we have found the RHF method much more stable than UHF for highly excited states. The possible mixing of occupied and unoccupied states in UHF solutions often results in convergence to a state of lower energy. In the discussion of results presented below, we will be careful to label which HF method was used to obtain the presented numbers.

TABLE VI. RHF energies for excited He $M=-1$ states, in hartree. The results from Thurner *et al.* [13], are given by E_{Th}.

	$1s3p_{-1}$		$1s3d_{-1}$	
β_Z	$-E_{RHF}$	$-E_{Th}$	$-E_{RHF}$	$-E_{Th}$
0.0000	2.0576		2.0556	
0.0001	2.0588	2.0588	2.0568	2.0568
0.0005	2.0633	2.0633	2.0614	2.0614
0.0010	2.0685	2.0685	2.0670	2.0670
0.0030	2.0851	2.0851	2.0869	2.0868
0.0070	2.1078	2.1054	2.1196	2.1187
0.0100	2.1208	2.1149	2.1408	2.1387
0.0300	2.2044	2.1332	2.2548	2.2384
0.0500	2.2839		2.3508	2.3131
0.0700	2.3686		2.4366	2.3755
0.1000	2.4812		2.5525	2.4540
0.1200	2.5500		2.6257	
0.1400	2.6110		2.6913	
0.1600	2.6739		2.7575	
0.1800	2.7356		2.8188	
0.2000	2.7936		2.8741	2.6348
0.2200	2.8438		2.9331	
0.2400	2.8984		2.9968	
0.2600	2.9507		3.0496	
0.2800	2.9931		3.1061	
0.3000	3.0357		3.1559	2.7358
0.4000	3.2699		3.4004	
0.5000	3.4663	2.8952	3.6053	3.0261
0.6000	3.6441		3.7845	
0.7000	3.8099	3.2998	3.9507	3.4405
0.8000	3.9561		4.0919	
0.9000	4.0838		4.2235	
1.0000	4.2065	3.7853	4.3470	3.9355

TABLE VII. RHF energies for excited He $M=-2$ and $M=-3$ states, in hartree. The results from Thurner *et al.* [13], are given by E_{Th}. Note that, for $\beta_Z=0.0001$, the value of E_{Th} for the $1s3d_{-2}$ state is considerably lower than E_{RHF}. A discontinuity in the slope of the E_{Th} data at $\beta_Z=0.0001$ shows that this value is in error.

	$1s3d_{-2}$		$1s4f_{-2}$		$1s4f_{-3}$	
β_Z	$-E_{RHF}$	$-E_{Th}$	$-E_{RHF}$	$-E_{Th}$	$-E_{RHF}$	$-E_{Th}$
0.0000	2.0556		2.0313		2.0313	
0.0001	2.0572	2.0578	2.0328	2.0328	2.0332	2.0332
0.0005	2.0634	2.0634	2.0388	2.0388	2.0406	2.0406
0.0010	2.0707	2.0707	2.0455	2.0455	2.0489	2.0489
0.0030	2.0968	2.0967	2.0666	2.0666	2.0753	2.0753
0.0070	2.1390	2.1387	2.0965	2.0973	2.1157	2.1151
0.0100	2.1663	2.1655	2.1197	2.1159	2.1412	2.1400
0.0300	2.3110	2.3063	2.2212	2.2063	2.2783	2.2700
0.0500	2.4310	2.4194	2.3118	2.2728	2.3916	2.3747
0.0700	2.5380	2.5193	2.4063	2.3278	2.4938	2.4671
0.1000	2.6824	2.6532	2.5253	2.3958	2.6344	2.5907
0.1200	2.7675		2.5928		2.7208	
0.1400	2.8446		2.6616		2.8022	
0.1600	2.9223		2.7263		2.8809	
0.1800	3.0019		2.7957		2.9551	
0.2000	3.0801	3.0146	2.8503	2.5447	3.0270	2.9222
0.2200	3.1656		2.9184		3.0955	
0.2400	3.2326		2.9721		3.1611	
0.2600	3.2959		3.0250		3.2246	
0.2800	3.3556		3.0837		3.2871	
0.3000	3.4121	3.2929	3.1347	2.6170	3.3484	3.1753
0.4000	3.6961		3.3691		3.6235	
0.5000	3.9611	3.7016	3.5648	2.9874	3.8689	3.5421
0.6000	4.1664		3.7489		4.0914	
0.7000	4.3600	3.9871	3.9155	3.4024	4.2853	3.7930
0.8000	4.5429		4.0714		4.4590	
0.9000	4.7069		4.2050		4.6322	
1.0000	4.8724	4.5145	4.3398	3.8987	4.7802	4.3488

III. APPLICATION TO SMALL ATOMS

A. Ground state and low-lying excitations

Tables I–IV contain the total energy as a function of magnetic field strength for the low-lying electronic states of H^-, He, Li, and C. We also list, for H^- and He, the results from other methods of calculation. For Li and C no comparisons are made, as we have found no computations performed in this range of magnetic fields for atoms with more than two electrons. As far as we know, these are the first calculations for these atoms for intermediate magnetic field strengths.

We wish to understand the spectral properties of light atoms in this range of magnetic fields, where many astrophysical applications can be found. Figures 1–3, therefore, show the computed energy spectrum for all of the atoms that we have considered thus far. Figure 1 shows the results listed in Tables I and II for low-lying excitations of H^- and He. The HF calculations of Thurner *et al.* [13], E_{Th}, are always slightly higher than the present results. This discrepancy is due to the ansatz used in the Thurner *et al.* method, where the wave function was expanded in spherical harmonics for small fields, and Landau-like orbitals for large fields. The two expansions meet in the intermediate range of field strength. Note that the H^- comparison between the two HF methods, shown in Fig. 1, demonstrates that the results of Thurner *et al.* are getting better as the field increases. The convergence of the two HF methods as we enter the superstrong regime is expected, since the assumption of cylindrical symmetry becomes more accurate as we approach the adiabatic regime. The variational energies of Larsen [16], E_{Lar}, which include electron correlation, are slightly lower than our HF numbers, as expected, and match very well with previous QMC calculations [22], which used HF trial wave functions. Note that HF does not obtain the correct ground state for H^- at small fields. The electron correlation (the difference between the HF and the exact energies) is sufficiently large to reorder the spin singlet and triplet states. At zero field, it has been shown that H^- has only a single bound state [23], while in nonzero fields (even infinitesimally small), there are an infinite number of bound states [24]. This sudden plethora of bound states arises from the fact that the constant field pins the extra electron, and thus enhances the attraction between the neutral atom and the additional electron. The QMC results for the $1s^2$ state are exact, due to the bosonic nature of the spatial component of the singlet wave function.

The case of He, a second benchmark of our calculations, is also shown in Fig. 1, where we again compare our results with those of Thurner *et al.*, Larsen, and the QMC calculations. Again, note that the asymptotic expansion HF approach is clearly inferior to our calculations, and again improves as the field strength gets very large, near $\beta_Z \geq 1$. Also note that the correlation energy is much larger for the singlet state than for the triplet, since the singlet state is much more compact than the triplet. We will consider more highly excited states for neutral He in the next section.

As one would expect, as the field is increased, the ground state of the system becomes spin polarized in order to minimize the Zeeman energy, and reduce electron repulsion. For the two electron systems considered thus far, there has been only one such transition, from a spin singlet ($S=0$) to a spin triplet ($S=1$). This transition occurs near $\beta_Z \simeq 0.02$ for H^- and $\beta_Z \simeq 0.1$ for He, and is also a transition in L_z, but not in z parity. This type of transition is not difficult to understand. As the field gets larger, the system tends to shrink, and by raising the angular momentum of the most exterior electron, the atom is able to increase the electronic separation. Figure 2 shows the energy of the first four electronic states of neutral Li. In this case there are two transitions, the first near $\beta_Z \simeq 0.01$ is a transition to a state of lower Zeeman energy ($M=0$ to $M=-1$, Π_z unchanged, and S_z unchanged), while the second, near $\beta_Z \simeq 0.16$, is the expected transition to a completely spin polarized state (M is unchanged, but $\Pi_z=+1$ to $\Pi_z=-1$, and $S_z=-1/2$ to $S_z=-3/2$). A similar plot can be drawn for C, also shown in Fig. 2. In the case of C, however, there are two spin transitions. The first, near $\beta_Z \simeq 0.005$, from $S_z=-1$ to $S_z=-2$ (with $M=-1$ to $M=-2$, and Π_z from -1 to $+1$), and the second, at $\beta_Z \simeq 0.18$, to the completely spin polarized state, $S_z=-3$ (with both M and Π_z unchanged). Figure 4 displays the ground-state quantum numbers for the entire series of transitions, as determined by our calculations. As the field is increased, the spatial extent of the ground states for these atoms becomes smaller, and there is a competition between the mutual repulsion of the electrons and the Zeeman energy. Just as for the two electron systems, the larger atoms increase the rotational energy of the electrons in order to decrease the electron repulsion. Figure 5 shows the electron density profiles for the ground state of each atom at several different values of the field strength. Atoms that in small fields are almost spherically symmetric acquire very compact butterfly or needlelike shapes as the field strength increases. Also note the needlelike structure of the final completely

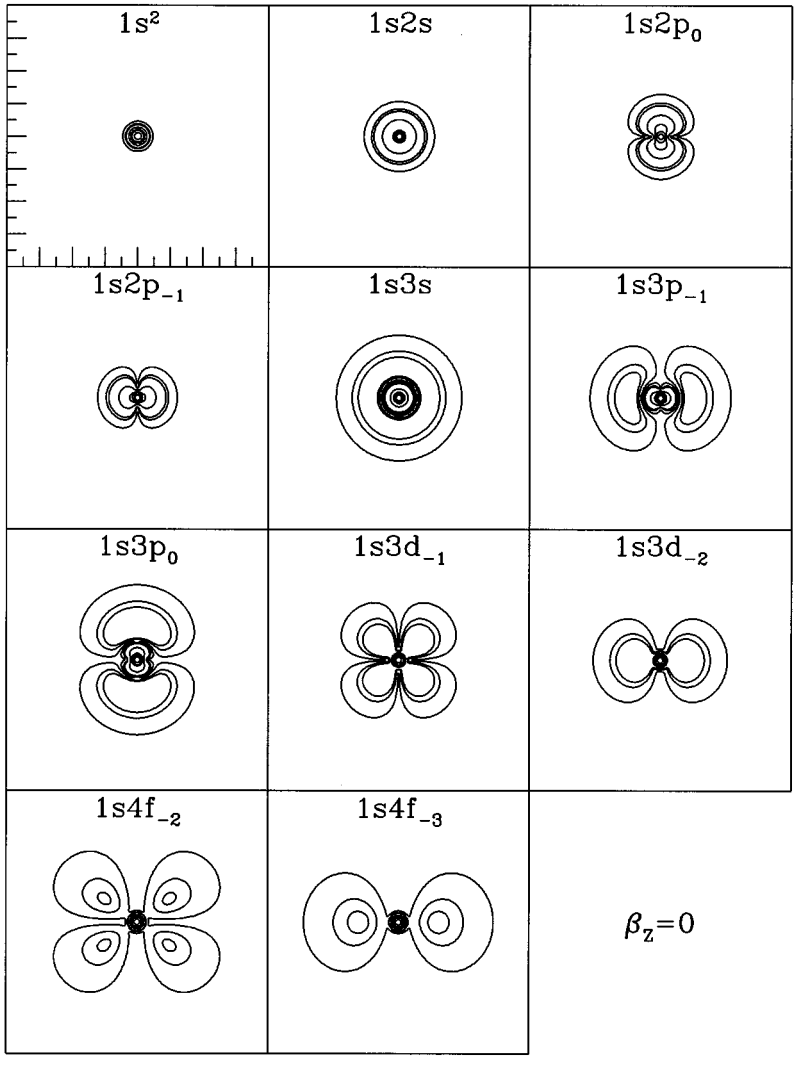

FIG. 6. Electronic density profiles for various He excitations at zero magnetic field. This figure is to be compared with Fig. 7, which shows the same density profile at a large applied field. The scale on both axes is the same, and corresponds to $-40a_0 \leq x,z \leq 40a_0$. The ordering of the states with respect to energy is from left to right, top to bottom.

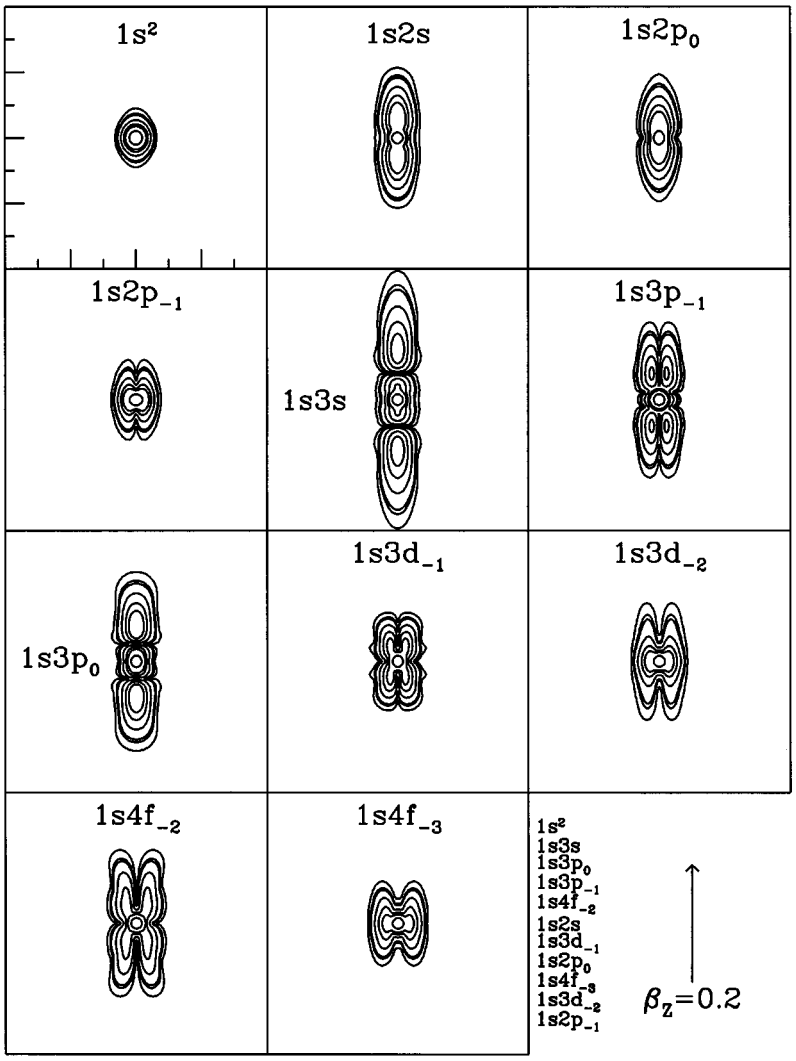

FIG. 7. Electronic density profiles for the helium excitation spectrum at $\beta_Z=0.2$. The same density values are contoured as in Fig. 6, but the scale is twice as small, from $-20a_0$ to $20a_0$. The correct ordering of the states according to variational energy is given by the key in the bottom right panel, with the $1s2p_{-1}$ state as the lowest, and the $1s^2$ state as the highest.

spin-polarized ground state at the largest magnetic field value for each atom.

B. Spectrum of neutral He

Due to its importance in astrophysical settings, we present in Tables V–VII RHF energies for more highly excited states of neutral He. In Fig. 3 we compare these energies with the HF calculations of Thurner *et al.* [13]. Thurner *et al.*'s calculations have difficulty at intermediate field strength, whereas our STO basis set calculations are much more flexible. In Figs. 6 and 7 we compare the electronic density profiles for a series of excited states of He for $\beta_Z=0$ and $\beta_Z=0.2$. Note that the applied field has completely reordered the energy spectrum, as well as compressing the atom to less than half its zero field size.

A quantity which is more sensitive to deficiencies in the applied basis set is the derivative of the energy with respect to the magnetic field. Figure 8 shows the derivative of our variational energy as a function of field strength, as determined by the Hellman-Feynman theorem,

$$\partial E/\partial\beta_Z=\langle\Psi|\partial\hat{\mathrm{H}}/\partial\beta_Z|\Psi\rangle$$
$$=\langle Z^2(L_z+2S_z)+Z^4\beta_Z(x^2+y^2)\rangle_\Psi,$$

where Ψ is the HF many-body wave function (Slater determinant), and $\langle\mathscr{O}\rangle_\Psi$ is the expectation value of operator $\mathscr{O}$. Figure 8 considers two of the excited states of He, $1s2p_{-1}$ and $1s3p_{-1}$, in comparison with that taken from the results of Thurner *et al.* Aside from the noise that originates with basis-set deficiencies, we note that the slope of our energy curves is generally lower than the HF numerical quadrature prediction, and the difference grows with more highly excited levels. This difference points out the fact that the asymptotic expansion HF method has a more difficult time representing the spatially extended excited states, but improves as the states shrink, further evidence that the asymptotic method is best used in the adiabatic field regime, with intermediate field strengths treated by a more flexible technique.

One issue that arises in working with STO (or similar) basis-set representations for the atomic wave function is the uncertain nature of convergence to the HF variational en-

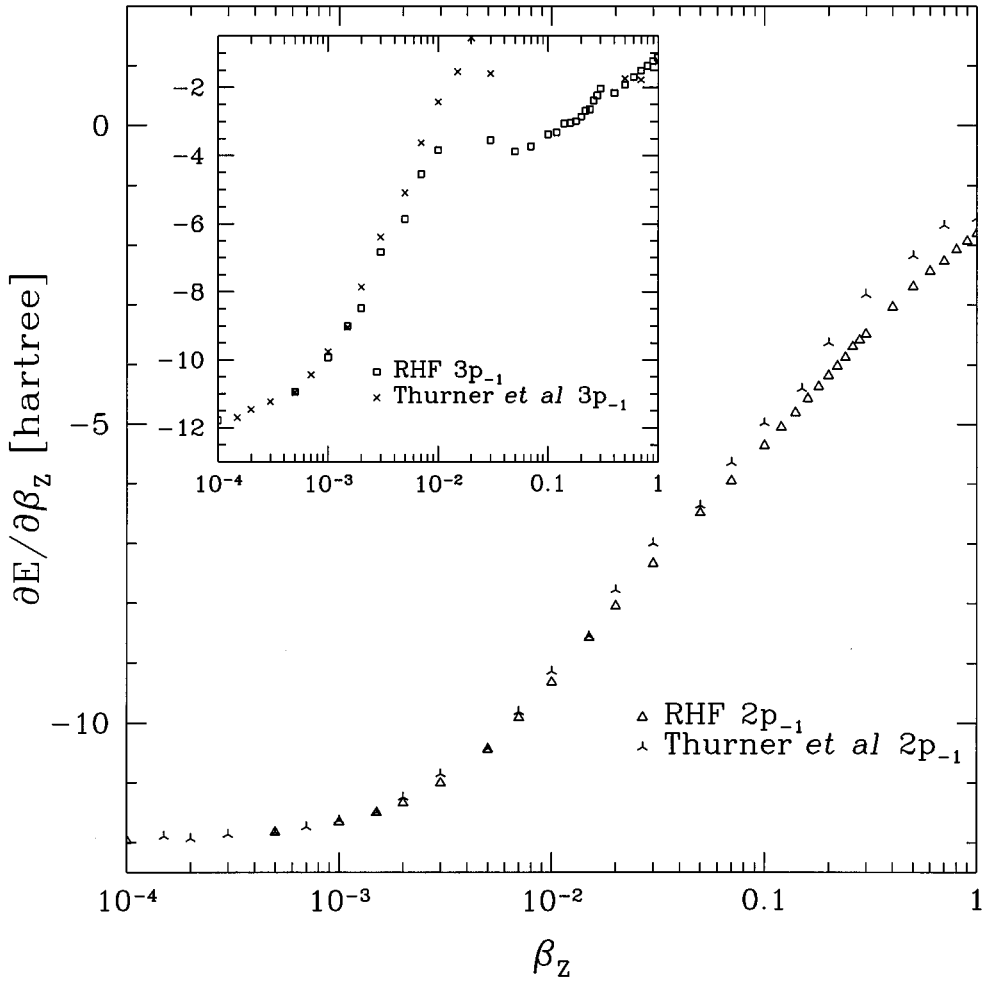

FIG. 8. The slope of the total energy curve is more sensitive to deficiencies in the HF approach. Here we compare the present results (open squares and triangles) with those of Thurner *et al.* [13], for the $2p_{-1}$ and $3p_{-1}$ states of He. Note the larger (in absolute value) slope for the present results. Irregularities in our data are caused by basis-set truncation.

ergy. Ideally, one simply adds more basis elements or optimizes the exponents of the basis further until a limiting value is achieved. In practice, however, one encounters limitations in the amount of resources available, either in time or computer memory. Figure 9 shows a typical set of calculations to get the lowest possible HF energy for the $1s2p_{-1}$ state of He at $\beta_Z=1$. Note that convergence is achieved when the number of basis elements, M, is greater than 35, and the maximum l used (in the spherical harmonics), L_{max}, is greater than 9. For more highly excited states (or outer shell electrons in larger atoms), one must generally increase L_{max} further, which also increases M. We have used $M \leqslant 70$ in all of our calculations, which introduces a truncation error. This truncation error increases with both Z and β_Z.

IV. SUMMARY AND CONCLUSIONS

We have presented a series of HF calculations of ground- and excited-state properties for selected first-row neutral atoms and negative ions in magnetic fields in excess of 10^{10} G, using a flexible STO basis set within the HF formalism. Oscillator strengths present no difficulty for this method, and are available upon request. Previous applications of the HF method to atoms in intermediate strength magnetic fields have been limited to hydrogen and helium, and have relied on numerical quadrature methods, resulting in higher energies and a less accurate wave function. The use of more general basis sets allows a greater flexibility in representing the atomic wave function as the magnetic field increases and the cylindrical symmetry associated with the magnetic field becomes important, and indeed, dominant.

Basis-set HF calculations, however, are not a panacea, since they suffer from several shortcomings. The most important disadvantage is the lack of certainty in the completeness of a basis set for a given calculation. The only systematic approach, and the one that we have used here, involves optimizing a set of basis elements with respect to the variational energy (the largest set that can be optimized in a reasonable length of time), then adding more elements until the energy no longer changes. The drawback of this approach is that one may end up in a local minimum of the energy surface, and not at the true HF result of lowest energy. Another disadvantage of using STO or similar basis sets is the non-negligible amount of computer time and memory required to diagonalize and store large matrices, whereas on a radial grid the matrices may be sparse. For atomic calculations in the absence of magnetic fields, numerical quadrature is generally simpler and more accurate. In the presence of strong magnetic fields, however, the flexibility of a basis-set approach is unparalleled.

Future efforts will use these accurate HF wave functions as the starting point for a series of quantum Monte Carlo (QMC) calculations on small atoms in strong magnetic fields, for which we will examine the behavior of electron

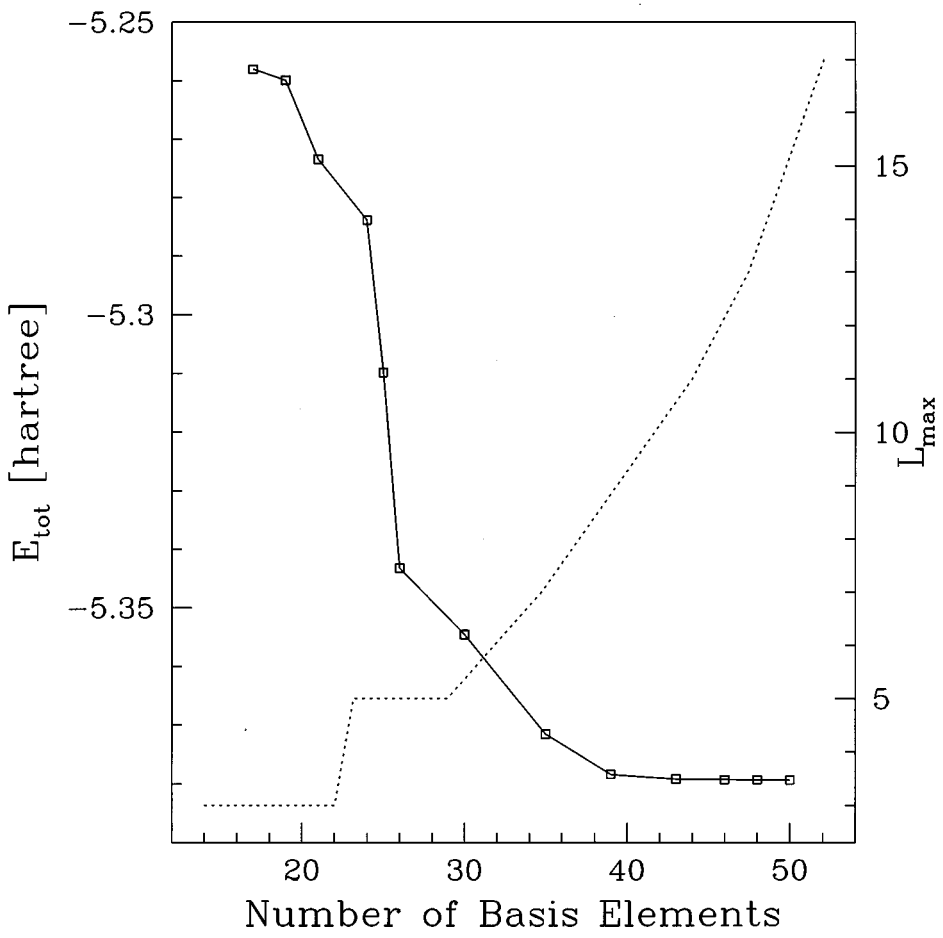

FIG. 9. The convergence of the variational energy (solid line) as a function of the size of the basis, for a typical data point, in this case for the $1s2p_{-1}$ state of He at $\beta_Z=1$. The dashed line indicates the largest l value used in the basis-set expansion.

correlation as a function of magnetic field strength and atomic number. These efforts are part of a project to develop exchange-correlation functionals in the context of current-density functional theory [25].

ACKNOWLEDGMENTS

This work was supported by NSF Grant No. DMR-91-17822 and ONR Grant No. N00014-93-1029.

APPENDIX: ELECTRON-ELECTRON MATRIX ELEMENT

We now consider the form of our matrix element for the electron-electron interaction matrix element in the STO basis. The usual approach [19] becomes numerically unstable at large values of l in the spherical harmonics $Y_{lm}(\theta,\phi)$, and is therefore inadequate for very strong fields. One can instead use a numerical evaluation of the integral which is inherently stable for most reasonable choices of basis elements.

The electron-electron matrix element in the STO basis is given by

$$I^{ee}_{\mu\nu\lambda\sigma}=\int dV_1 dV_2 \chi_\mu(\mathbf{r}_1)\chi_\nu(\mathbf{r}_1)r_{12}^{-1}\chi_\lambda(\mathbf{r}_2)\chi_\sigma(\mathbf{r}_2), \tag{A1}$$

where $\chi_\mu=R_\mu(r)Y_{l_\mu m_\mu}(\theta,\phi)$, r_{12} is the interelectron distance, $R_\mu(r)=N_\mu r^{n_\mu-1}e^{-a_\mu r}$, and $N_\mu=[(2a_\mu)^{(2n_\mu+1)}/(2n_\mu)!]^{1/2}$ is the normalization factor for basis element μ. We expand the interelectron distance in terms of spherical harmonics and perform the angular integrals, yielding

$$I^{ee}_{\mu\nu\lambda\sigma}=\sum_{l\epsilon S_\Omega} I^l_\Omega (G^l_{\mu\nu\lambda\sigma}+G^l_{\lambda\sigma\mu\nu}), \tag{A2}$$

$$G^l_{\mu\nu\lambda\sigma}=\int_0^\infty u^{1-l}R_\mu(u)R_\nu(u)du\int_0^u v^{2+l}R_\lambda(v)R_\sigma(v)dv, \tag{A3}$$

where

$$S_\Omega=\{|l_\mu-l_\nu|,|l_\mu-l_\nu|+2,\ldots,l_\mu+l_\nu\} \cap\{|l_\lambda-l_\sigma|,|l_\lambda-l_\sigma|+2,\ldots,l_\lambda+l_\sigma\}, \tag{A4}$$

is the set of l values over which we need to sum, and

$$\begin{aligned} I^l_\Omega=(-1)^{m_\mu+m_\sigma}&\left[\frac{(2l_\mu+1)(2l_\nu+1)(2l_\lambda+1)(2l_\sigma+1)}{(2l+1)^4}\right]^{1/2} \\ &\times\langle l_\mu,l_\nu;0,0|l,0\rangle\langle l_\mu,l_\nu;-m_\mu,m_\nu|l,m_\nu-m_\mu\rangle \\ &\times\langle l_\lambda,l_\sigma;0,0|l,0\rangle \\ &\times\langle l_\lambda,l_\sigma;-m_\lambda,m_\sigma|l,m_\sigma-m_\lambda\rangle\,\delta_{m_\sigma-m_\lambda,m_\mu-m_\nu}, \end{aligned} \tag{A5}$$

is the value of the angular integrals for a given l, and $\langle l_1,l_2;m_1,m_2|l,m\rangle$ are Clebsch-Gordan coefficients. The Clebsch-Gordan coefficients may be tabulated for a given calculation, and present no difficulty, even for very large l.

The problem arises in evaluating the radial integrals in Eq. (A3) when the individual l's can be quite large. Changing variables on the inner integral, and using $t=(a_\lambda+a_\sigma)v$ yields a standard form,

$$G^l_{\mu\nu\lambda\sigma}=\overline{N}_{\mu\nu\lambda\sigma}\int_0^\infty u^{n_\mu+n_\nu-l-1}e^{-(a_\mu+a_\nu)u} \times\gamma(1+n_\lambda+n_\sigma+l,(a_\lambda+a_\sigma)u), \qquad \text{(A6)}$$

where γ is the incomplete gamma function and

$$\overline{N}_{\mu\nu\lambda\sigma}=\frac{N_\mu N_\nu N_\lambda N_\sigma}{(a_\lambda+a_\sigma)^{n_\lambda+n_\sigma+l+1}}. \qquad \text{(A7)}$$

The integral in Eq. (16) is in standard tables [26]. Let $m=n_\mu+n_\nu-l$, $n=1+l+n_\lambda+n_\sigma$, $\alpha=a_\lambda+a_\sigma$, and $\beta=a_\mu+a_\nu$. The radial integral can now be expressed in terms of a confluent hypergeometric function, ${}_2F_1$,

$$G^l_{\mu\nu\lambda\sigma}=\overline{N}_{\mu\nu\lambda\sigma}\frac{\alpha^m\Gamma(m+n)}{n(\alpha+\beta)^{m+n}} \times{}_2F_1(1,m+n;n+1;\alpha/(\alpha+\beta)), \qquad \text{(A8)}$$

where $\Gamma(i)=(i-1)!$ is the usual gamma function. For this particular application, it is actually advantageous to sum the hypergeometric function directly. After using the series expansion for ${}_2F_1$ and performing some algebraic manipulations, we obtain

$$G^l_{\mu\nu\lambda\sigma}=N_\mu N_\nu N_\lambda N_\sigma\frac{(n-1)!}{(\alpha+\beta)^{m+n}} \times\sum_{k=0}^{\infty}\frac{(m+n+k-1)!}{(n+k)!}\left(\frac{\alpha}{\alpha+\beta}\right)^k. \qquad \text{(A9)}$$

In general the sum for a hypergeometric function may not converge, but for this situation the sum is well-behaved and convergent. In practice, one can express the terms in Eq. (19) recursively and quickly evaluate the sum to a desired tolerance.

[1] R. J. Elliott and R. Louden, J. Phys. Chem. Solids **15**, 196 (1960).
[2] H. Bethe and E. E. Salpeter, *Quantum Mechanics of One-And Two-Electron Systems* (Springer-Verlag, Berlin, 1957).
[3] Y. Wan, G. Ortiz, and P. Phillips, Phys. Rev. Lett. **75**, 2879 (1995).
[4] J. Trümper, W. Pietsch, C. Reppin, W. Voges, R. Stauben, and E. Kendziorra, Astrophys. J. **219**, L105 (1978).
[5] J. D. Landstreet, in *Cosmical Magnetism*, edited by D. Lynden-Bell (Kluwer, Boston, 1994), p. 55.
[6] L. I. Schiff and H. Snyder, Phys. Rev. **55**, 59 (1939).
[7] W. Rosner, G. Wunner, H. Herold, and H. Ruder, J. Phys. B **17**, 29 (1984).
[8] H. Ruder, G. Wunner, H. Herold, and F. Geyer, *Atoms in Strong Magnetic Fields* (Springer, Berlin, 1994).
[9] R. O. Mueller, A. R. P. Rao, and L. Spruch, Phys. Rev. A **11**, 789 (1975).
[10] M. Vincke and D. Baye, J. Phys. B **22**, 2089 (1989).
[11] M. C. Miller and D. Neuhauser, Mon. Not. R. Astron. Soc. **253**, 107(1991).
[12] D. Neuhauser, S. E. Koonin, and K. Langanke, Phys. Rev. A **33**, 2084 (1986); **36**, 4163 (1987).
[13] G. Thurner, H. Korbel, M. Braun, H. Herold, H. Ruder, and G. Wunner, J. Phys. B **26**, 4719 (1993).
[14] R. J. W. Henry, R. F. O'Connell, E. R. Smith, G. Chanmugam, and A. K. Rajagopal, Phys. Rev. D **9**, 329 (1974).
[15] G. L. Surmelian, R. J. W. Henry, and R. F. O'Connell, Phys. Lett. **49A**, 431 (1974).
[16] D. M. Larsen, Phys. Rev. B **20**, 5217 (1979).
[17] G. Ortiz, M. D. Jones, and D. M. Ceperley, Phys. Rev. A **52**, 3405 (1995).
[18] G. D. Schmidt, W. B. Latter, and C. B. Foltz, Astrophys. J. **350**, 758 (1990).
[19] C. C. J. Roothaan, Rev. Mod. Phys. **23**, 69 (1951).
[20] R. McWeeny, *Methods of Molecular Quantum Mechanics* (Academic, New York, 1992), Chap. 6.
[21] M. F. Guest and V. R. Saunders, Mol. Phys. **28**, 819 (1974).
[22] M. D. Jones and G. Ortiz (unpublished).
[23] R. N. Hill, Phys. Rev. Lett. **38**, 643 (1977).
[24] J. E. Avron, I. W. Herbst, and B. Simon, Commun. Math. Phys. **79**, 529 (1981).
[25] G. Vignale and H. Rasolt, Phys. Rev. Lett. **59**, 2360 1987.
[26] I. S. Gradshteyn and I. M. Ryzhik, *Tables of Integrals, Series, and Products* (Academic, New York, 1980), p. 663.